Theoretical Study on the Application of a Janus CoSTe Monolayer for Li-S Batteries

Xinzhu Wen[1] · Fengsheng Zeng[1] · Feng Shao[2] · Hong Li[1]

Abstract

Li-S batteries show great promise for next-generation energy systems but suffer from sluggish reaction kinetics and the inevitable "shuttling effect" of dissolved lithium polysulfides (LiPSs). In this study, a structure model of a Janus CoSTe monolayer is constructed is to investigate the adsorption energy with LiPSs, adsorption decomposition energy, and diffusion barrier on Li_2S for Li-S batteries. The results show that the adsorption energy of Li_2S_n clusters on the surface of Janus CoSTe monolayers is much higher than that of graphite and organic electrolyte, and the decomposition of Li_2S_n clusters cannot easily occur on the Janus CoSTe monolayer. Moreover, the diffusion of Li_2S_n clusters on the surface of Janus CoSTe monolayers has its microscopic "channel", leading to the low dissociation energy of Li_2S. Theoretically, the Janus CoSTe monolayer exhibits excellent catalytic capability for lithium-sulfur batteries and shows great potential to be an excellent anchoring material for high-performance Li-S batteries.

Keywords First-principles · shuttle effect · Janus CoSTe monolayer · lithium-sulfur batteries · catalytic capability

Introduction

Compared with lithium-ion batteries, lithium-sulfur batteries have high theoretical capacity (1672 mA h/g) and theoretical specific energy density (2600 W h/kg). As a high-capacity, low-cost and environmentally friendly secondary battery, the research on lithium-sulfur batteries has developed rapidly recently and they are expected to replace lithium-ion batteries.[1–3] However, there are many problems that must be solved for large-scale commercialization and practical application of lithium-sulfur batteries.[2,4–6] (1) the poor conductivity of sulfur and its discharge products Li_2S and Li_2S_2, (2) the "shuttle effect" of the dissolved polysulfides, which

✉ Xinzhu Wen
    wxz123@yeu.edu.cn

✉ Hong Li
    melihong@sjtu.edu.cn

1   Institute of Engineering and Technology, Yang en University, Quanzhou 362014, Fujian, People's Republic of China

2   Key Laboratory for Thin Film and Microfabrication Technology of the Ministry of Education, School of Electronics, Information and Electrical Engineering, Shanghai Jiao Tong University, Dong Chuan Road No.800, Shanghai 200240, People's Republic of China

is the main reason for the rapid decrease in efficiency and capacity,[7] and (3) the large volume expansion between sulfur cathode and its discharge products.[2] In order to solve the above problems, strategies have been proposed to overcome these obstacles by developing strong polar host materials, new electrolytes and anodic protection methods.[8,9] So far, an effective method is to capture and catalyze the dissolved Li_2S_n intermediate by using polar materials.[10,11] A catalyst with good conductivity and high polarity can restrain the shuttle effect and greatly improve the cycle life of lithium-sulfur batteries.[12,13] Metal oxygen/sulfide composites such as mesoporous TiO_2 spheres have large pore volume, which provides an abundant reaction interface for internal electrochemistry and accelerates electron transport.[14] Hydrophilic MgO nanoparticles with hydroxyl groups can chemically inhibit the dissolution of polysulfides,[15] and ultra-fine Nb_2O_5 nanocrystals can effectively reduce the loss of active sulfur by the strong physical and chemical interactions with Li_2S_n.[16] Moreover, Xu et al. found that Te can effectively capture Li_2S_n in lithium-sulfur batteries.[17]

Recently, a new class of so-called Janus transition metal disulfides (Janus TMDs) has aroused widespread interest because of their special sandwich structure, in which the top and bottom atomic layers are composed of different chalcogen atoms. Changing the structural symmetry of the two

sides of TMDs can adjust the electric dipole distance, carrier mobility, magnetism, valley polarization and band gap.[18] In this study, the Janus CoSTe monolayer is constructed to study the adsorption energy with Li_2S_n, decomposition energy, diffusion energy and the Gibbs free energy evolution of each reaction step of sulfur reduction. All results show that the Janus CoSTe monolayer is a potential anchoring material for high-performance of lithium-sulfur batteries.

Stability and Calculation Method of Calculation Model

The Janus CoSTe monolayer is modeled with a $4 \times 4 \times 1$ supercell with 16 S, Te and Co atoms. The layer is set to 20 Å along the Z direction to eliminate the minor interaction. As shown in the top and the side view (Fig. 1a), the single-atom formation energy of Janus CoSTe monolayer is calculated to be -0.72 eV, based on the equation: $E_f = (E_{CoSTe} - \sum n_i E_i)/N$. In the formula, E_f, E_{CoSTe} represents the formation energy of a single atom and the total energy of Janus CoSTe film, respectively, $\sum n_i E_i$ represents the sum of Gibbs free energy of all individual atoms, and N represents the total number of atoms in the structure. The molecular dynamics (MD) of the Janus CoSTe monolayer under constant particle number, volume and temperature (NVT) ensemble was simulated by the Forcite tool and NOSE algorithm, and its thermal stability at room temperature was determined. The object is a $4 \times 4 \times 1$ supercell, and the total time and time step are set to 5000 ps and 1 fs, respectively. Figure 2a shows the fluctuation of the total energy of the Janus CoSTe monolayer. Its total energy oscillation is maintained in a narrow fluctuation range (< 1.5 eV) and there is no bond breaking or structural deformation during the MD simulation animation (see supplementary materials). Figure 2b shows the phonon spectrum of the unit structure of the CoSTe monolayer. It can be seen that there is no imaginary frequency in the phonon spectrum. These results show that the Janus CoSTe monolayer is stable and can be tested at room temperature.

The density functional theory calculation is performed using the Cambridge Sequential Total Energy Package (CASTEP)[19] and the generalized gradient approximation (GGA)[20,21] with Perdew–Burke–Ernzerhof (PBE) exchange-correlation functional.[22] The geometric structure is optimized by the Broyden–Fletcher–Goldfarb–Shanno (BFGS) algorithm,[23,24] and the ultra-soft pseudopotential is used to describe electron-ion interaction. The specific electronic configurations are Te (5s2 5p4), Co (4s2 3d7). S (3s2 3p4), the d orbitals of the transition metal element Co are
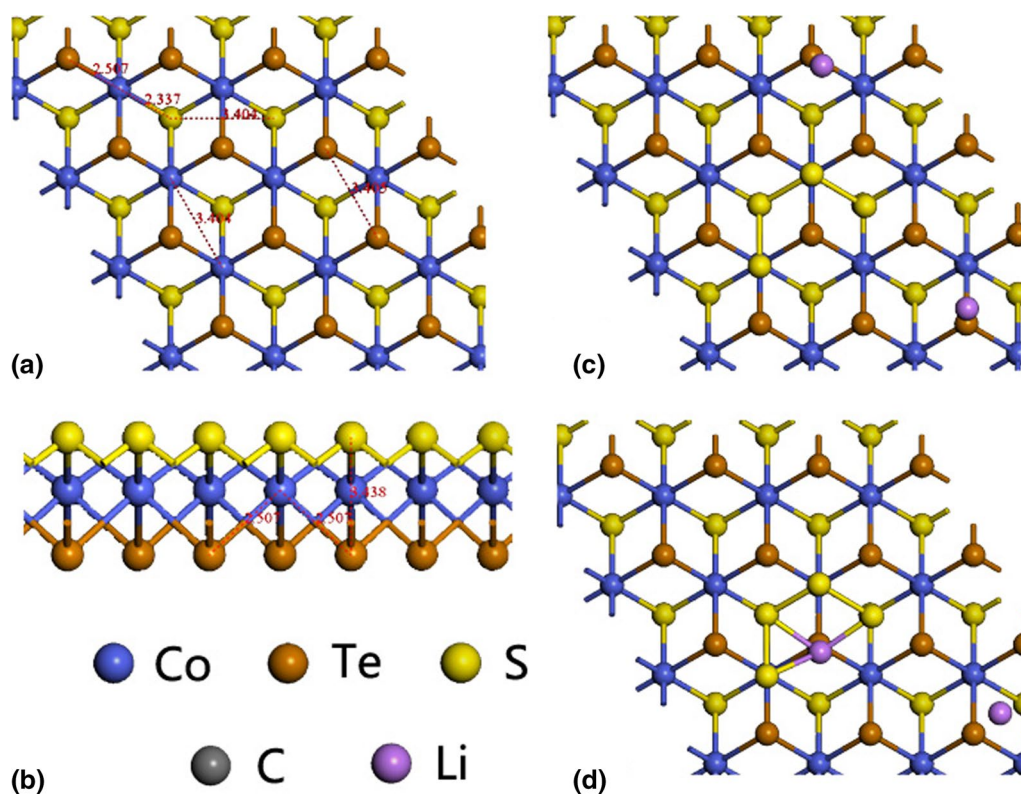

Fig. 1 (a) CoSTe monolayer top view, (b) side view, (c) CoSTe monolayer Te surface $Li + Li + S_4$ coadsorption diagram, (d) CoSTe monolayer Te surface $Li + LiS_4$ coadsorption diagram.
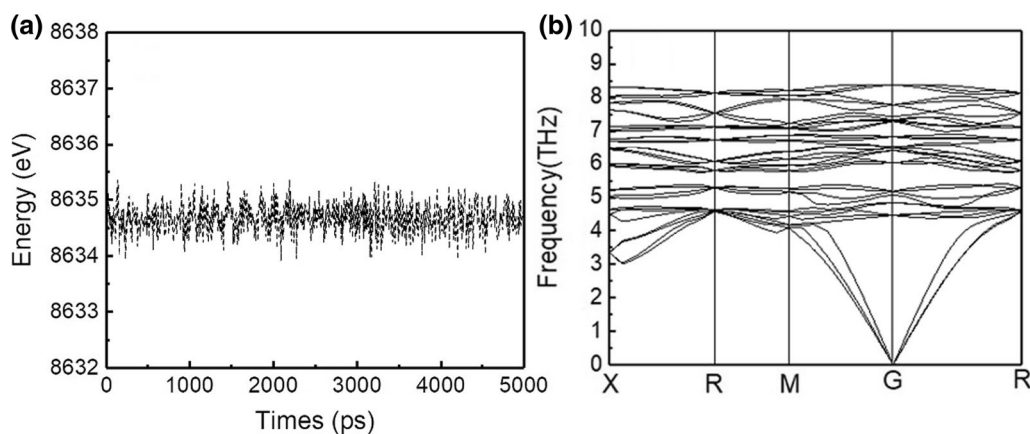
Fig. 2 (a) Total energy fluctuation simulated by the molecular dynamics of the Janus CoSTe monolayer at 298 K. (b) Phonon spectrum of the unit structure of the CoSTe monolayer.

Table I Data of S/Te surface adsorption configuration and adsorption energy

Surface		S_8	Li_2S_8	Li_2S_6	Li_2S_4	Li_2S_2	Li_2S
Te	$\Delta d_{(Li\text{-}S)}$(Å)	–	0.018	0.032	0.059	0.223	0.235
	h_{Smin}(Å)	2.862	2.949	3.074	2.773	2.702	2.627
	h_{Limin}(Å)	–	2.470	2.482	2.508	1.615	1.564
	E_{ads}(eV)	0.88	1.41	1.44	1.86	2.37	2.85
	E_{vdw}(eV)	0.82	0.95	0.84	0.76	0.59	0.42
S	$\Delta d_{(Li\text{-}S)}$ (Å)	–	0.005	0.009	0.042	0.123	0.165
	h_{Smin}(Å)	2.645	2.540	2.512	2.510	2.340	2.325
	h_{Limin}(Å)	–	3.731	3.820	2.421	2.284	2.175
	E_{ads}(eV)	1.32	1.93	2.04	2.02	2.45	2.70
	E_{vdw}(eV)	1.26	1.58	1.55	1.21	1.10	0.86

corrected by Hub U ($U=2.5$ eV),[25] and the van der Waals remote weak interaction correction uses the Grimme DFT-D3 method.[26] The plane wave energy cut-off is set to 420 eV, the Brillouin zone integral of structural optimization adopts $4\times4\times1$ K-point sampling centered on the G-point, and $8\times8\times1$ K-point sampling is used in all energy calculations. The convergence standard of the self-consistent optimization of the structure is set as follows: the maximum displacement is 5.0×10^{-4} nm, the maximum internal stress is 0.02 Gpa, the maximum interaction force between atoms is 0.01 eV/nm, and the overall energy convergence of the structure is less than 5×10^{-6} eV/atom.

Results and Discussion

Adsorption of Li_2S_n Clusters on the Surface of the Janus CoSTe Monolayer

The chemical interaction between the Janus CoSTe monolayer and Li_2S_n is evaluated by the calculation of adsorption energy. Because of the heterogeneity of the two sides of the

Janus CoSTe monolayer, the adsorption energies of S_8 and Li_2S_n on the two surfaces are calculated, respectively, and the adsorption energy is calculated based on the equation $E_{ads} = E_{total} - E_{CoSTe} - E_{Li_2sn}$, where E_{CoSTe} and E_{Li_2sn} represent the optimal structure of Janus CoSTe monolayer and the energies of surface with corresponding Li_2S_n groups, respectively. E_{total} is the total energy of the optimal structure system adsorbed by Li_2S_n clusters. Some key data for the calculation of the two surfaces of the monolayer are presented in Table I. The final adsorption energy of S_8 and Li_2S_n on the two surfaces are shown in Fig. 3. The calculated results are also compared with the graphite surface (001) and the current mainstream electrolyte 1–3 dioxane (DOL), ethylene glycol dimethyl ether (DME) with the adsorption energy of polysulfides.[27] It is worth noting that the adsorption of S_8 on the S and Te surfaces of the monolayer is much higher than that in the electrolyte, so S_8 precipitates more easily on the S surface of the monolayer during charging.

Combined with the data of Fig. 4 and Table I, further analysis shows that the adsorption energy of the S surface ranges from 1.93 eV to 2.70 eV, and the low adsorption energy (E_{vdw}: E_{vdw} calculation uses the TS method in the
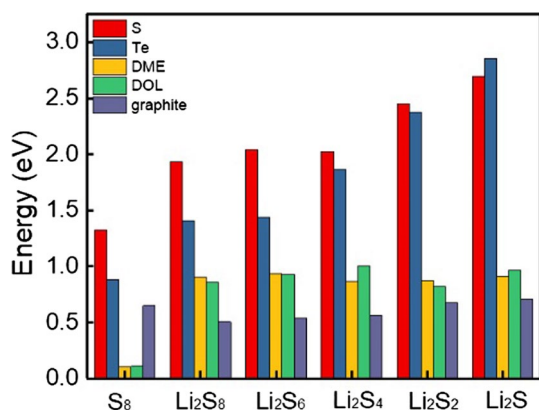
**Fig. 3** Adsorption energy of S_8 and Li_2S_n on S/Te/graphite surface with DME/DOL electrolyte.

DFT-D module and the semi-empirical data table to correct the dispersion directly) decreases from 1.26 eV to 0.86 eV. After adsorption, the change of Li-S bond length Δd in Li_2S_n clusters increases from 0.005 Å to 0.165 Å; the minimum adsorption height of S atoms to substrate in Li_2S_n clusters h_{Smin} decreases from 2.540 Å to 2.235 Å, and the minimum adsorption height of Li atoms to substrate decreases from 3.731 Å to 2.175 Å. It is clear to see that the adsorption energy is positively related to the change of Li-S bond length Δd. It is inversely related to the minimum adsorption height of S atoms in Li_2S_n clusters to the substrate h_{Smin}. On the other hand, the adsorption energy on the Te surface changes from 1.41 eV to 2.85 eV, in which the adsorption energy E_{vdw} decreases from 0.82 eV to 0.42 eV. The Li-S bond length in the Li_2S_n cluster changes from 0.018 Å to 0.235 Å, and the minimum adsorption height of the S atom to the substrate in the Li_2S_n cluster decreases from 2.949 Å to 2.627 Å. The minimum adsorption height of Li atoms to substrate (h_{Limin}) decreases from 2.470 Å to 1.564 Å. The change of adsorption energy is positively correlated with the change of Li–S bond length Δd, and has a greater reverse correlation with the minimum adsorption height of the Li atom to substrate h_{Limin}. The main reason for the above change is the intermolecular adsorption of cluster molecules on the S surface of the Janus CoSTe monolayer which is mainly based on the van der Waals force between the surface S and S in the cluster group. The longer interaction distance will lead to a stronger physical interaction, so the adsorption capacity of high-order Li_2S_n is greatly improved. With the decrease of Li_2S_n group, the number of S atoms in the cluster group decreases, and the proportion of physical adsorption becomes gradually less than the interaction between Li-S. Li_2S_n gets closer to the S surface, and the interaction between the S atom and the Li atom in the low-order Li_2S_n

is gradually enhanced, from the physical adsorption of high-order Li_2S_n to the chemical adsorption of Li-S bond of low-order Li_2S_n. The adsorption between the Te surface and Li_2S_n cluster group of the Janus CoSTe monolayer originates from the interaction between Te and Li. The shorter the adsorption distance, the higher of the chemical adsorption, so the adsorption capacity for low-order Li_2S_n is obviously enhanced. With the decrease of the number of S atoms in Li_2S_n, the distance between Li_2S_n and the Te surface decreases, and the interaction between Te atoms and the low-order small molecule Li_2S_n gradually increases. From the physical adsorption of high-order Li_2S_n to the chemical adsorption of the Li-Te bond of low-order Li_2S_n, the adsorption energy of Li_2S on the Te surface is higher than that on the S surface. Generally speaking, the S surface of the Janus CoSTe monolayer shows physical adsorption of sulfiphilicity, which is dominant in the adsorption of high-order Li_2S_n clusters, while the surface of Te shows chemical adsorption of lithiophilicity, which accounts for a higher proportion in the adsorption of low-order Li_2S_n clusters. The moderate adsorption of the Janus CoSTe monolayer can capture Li_2S_n more effectively than that of graphite and avoid the dissolution of high-order Li_2S_n in electrolyte, which is particularly important for the high performance of Li-S battery.

Decomposition of Li_2S_n Clusters on the Surface of Janus CoSTe Monolayers

Another property of the anchoring material that should be evaluated is whether the anchored Li_2S_n can be stable when adsorbed on the Janus CoSTe monolayer to prevent its decomposition and dissolution. Therefore, we have calculated the adsorption and decomposition energy of Li_2S_n on the two surfaces of the monolayer.[28] In the calculation method, the total energy of the Janus CoSTe monolayer with stable adsorption of Li_2S_n is defined as E_0, and two Li atoms are decomposed to the position sufficiently far from the S atom, generating the lowest energy structure of co-adsorption stability of $Li + LiS_n$ and $Li + Li + S_n$ on the surface of Janus CoSTe which is defined as E_1 and E_2, respectively. Figure 1c and d displays the $Li + LiS_4$ and $Li + Li + S_4$ co-adsorption diagrams of Li_2S_4 decomposition on the Te surface of the Janus CoSTe monolayer. By calculating the energy difference between intact structures and decomposed structures, $E_1 - E_0$ and $E_2 - E_0$, the surface Li atomic adsorption decomposition energies can be obtained, respectively. In terms of adsorption decomposition energy, whether on the S or Te surface, all the decomposition structures have positively correlated energy, indicating that the stability of complete Li_2S_n adsorption on the Janus CoSTe monolayer is higher than that after decomposition, so the decomposition

Fig. 4 Adsorption configuration of S_8 and Li_2S_n on the surface of the Janus CoSTe monolayer. (a) Final adsorption configuration on the S surface, (b) final adsorption configuration on the Te surface.
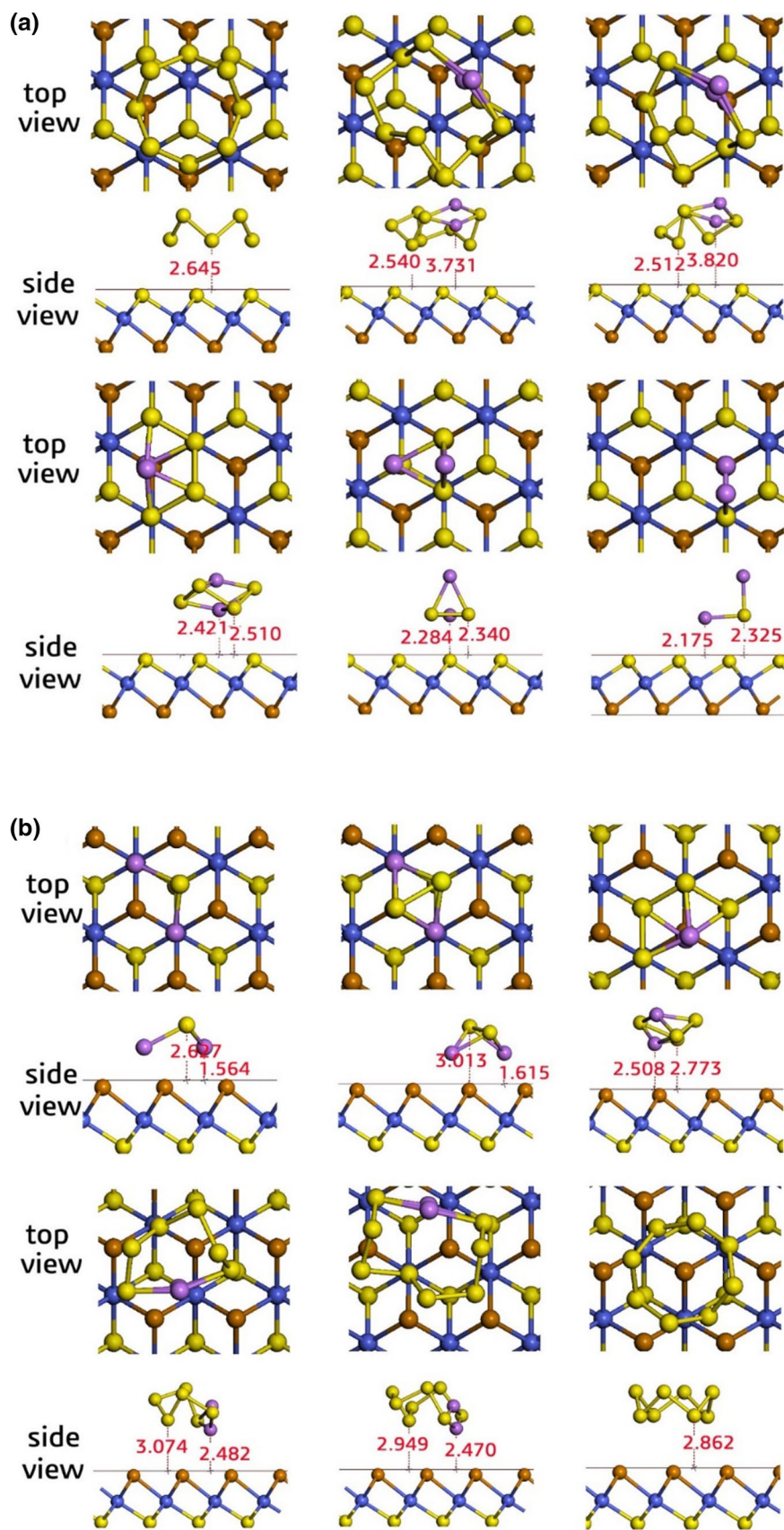
of Li_2S_n clusters does not easily occur spontaneously on the Janus CoSTe monolayer. The adsorption decomposition energy of high-order Li_2S_n clusters on S and Te surfaces of Janus CoSTe monolayers is significantly higher than that of low-order Li_2S_n. The decomposition energy of the S surface is slightly higher than that of the Te surface. Combined with the change of bond length (Table II), it is found that the larger the bond length of Li_2S_n, the smaller the adsorption decomposition energy. These results indicate that it is more difficult for the higher-order Li_2S_n to decompose than for low-order Li_2S_n. Moreover, the binding of Li-S in S-surface Li_2S_n is closer due to the change of Li-S bond in Li_2S_n caused by surface adsorption. So the effect of the Janus CoSTe film on inhibiting the decomposition of high-order Li_2S_n is greater than that of low-order Li_2S_n.

Li$_2$S Dissociation of Li$_2$S on the Surface of the Janus CoSTe Monolayer

Zhou et al. proposed that the Li_2S decomposition reaction barrier on the anchoring material surface is highly related to the overpotential measured in the experiment, and the surface delithiation reaction kinetics is very important to the overall performance of the Li-S battery. The larger the dissociation energy barrier, the higher the activation energy barrier needed for the activation of the initial electrode.[29] Therefore, the variation of the dissociation energy of Li_2S on the surface of the Janus CoSTe monolayer with the dissociation position is calculated, and the Li-S bond breaking reaction process of the dissociation path of Li atoms on S and Te surfaces of the Janus CoSTe monolayer is shown in Fig. 5a and b. The maximum height of the dissociation barrier on

Table II Adsorption decomposition energy of S/Te double sides of the Janus CoSTe monolayer

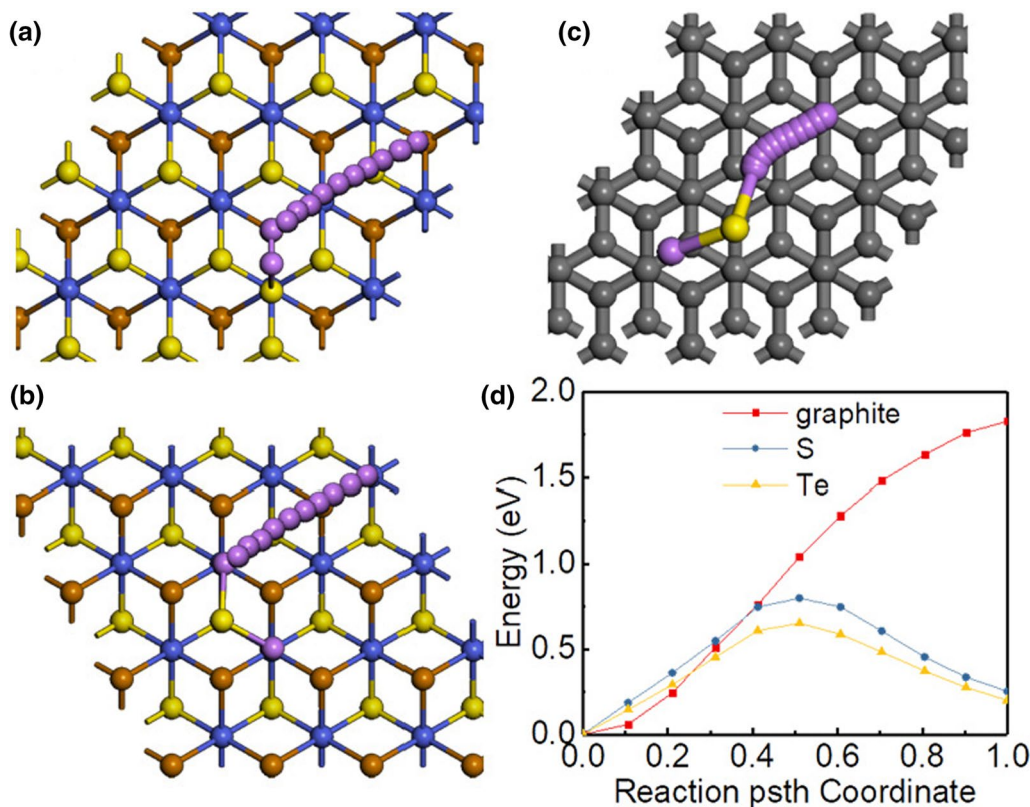| Surface	Energy	Li_2S_8	Li_2S_6	Li_2S_4	Li_2S_2	Li_2S
Te	E_1-E_0	2.18	1.86	1.81	0.84	0.38
	E_2-E_0	4.45	3.96	3.54	1.85	1.06
S	E_1-E_0	2.42	2.13	2.02	1.15	0.45
	E_2-E_0	4.87	4.29	3.95	2.98	1.23

Fig. 5 (a) Diffusion path of Li_2S on S surfaces, (b) Te surfaces, (c) graphite (C atoms are marked in grey in Fig. 1) surfaces, (d) dissociation energy of Li_2S on S, Te, graphite surfaces (Color figure online).

the Te surface is 0.67 eV. The maximum height of the dissociation barrier on the S surface is 0.74 eV, which is smaller than that on the graphite surface (1.81 eV). Combined with the previous data such as the change of bond length, it can be seen more clearly that the interaction between the Te surface and the Li atom on Li_2S is stronger than that on the S surface. In the process of decomposition, the radius of the Te atom is larger than that of the S atom, when the Li_2S (or Li_2S_n cluster) is at a certain height from the surface. The bonding effect of Li-Te is stronger than that of Li-S, and the effect of Te on reducing the dissociation barrier of Li_2S is better than that of the S surface. While compared with S and Te surfaces, the bonding effect of Li-C on the graphite surface is much weaker, so the decomposition process has a very large dissociation barrier.

Diffusion of Li_2S_n Clusters on the Surface of the Janus CoSTe Monolayer

The diffusion behavior of Li_2S_n clusters on the anchoring materials plays an important role in the performance of Li-S batteries. As shown in Fig. 6a and b, the diffusion energy barriers of Li_2S_n in Janus CoSTe monolayers on different surfaces are calculated. The minimum

energy path (MEP) is used to calculate the diffusion energy barrier: firstly, the complete LST/QST method is used to search the transition states in different diffusion paths, and then the fine-tuned nudged elastic band (NEB) method is used to calculate the free energy.[30] The diffusion coefficient (D) of Li_2S_n clusters on the surface can be calculated from the diffusion energy barrier according to the Arrhenius equation: $D = \exp(-E_d/k_B T)$, where E_a is the calculated energy barrier and k_B and T are the Boltzmann constant and ambient temperature, respectively. The diffusion energy barriers of Li_2S_n clusters on two surfaces and the diffusion coefficient ratios of different paths are summarized in Table III. The results show that the difficulty of Li atom diffusion in different directions on the surface of Janus CoSTe monolayer is generally the same, while for the corresponding Li_2S_n clusters in the same path, the diffusion energy barrier on the S surface is lower than that on the Te surface, indicating that the diffusion of Li_2S_n clusters on the S surface of the Janus CoSTe monolayer is easier on the Te surface. The diffusion energy barrier of Li_2S_n clusters increases rapidly with the increase of n, which indicates that the diffusion of high-order Li_2S_n clusters is much more difficult than that of low-order Li_2S_n clusters. The diffusion energy
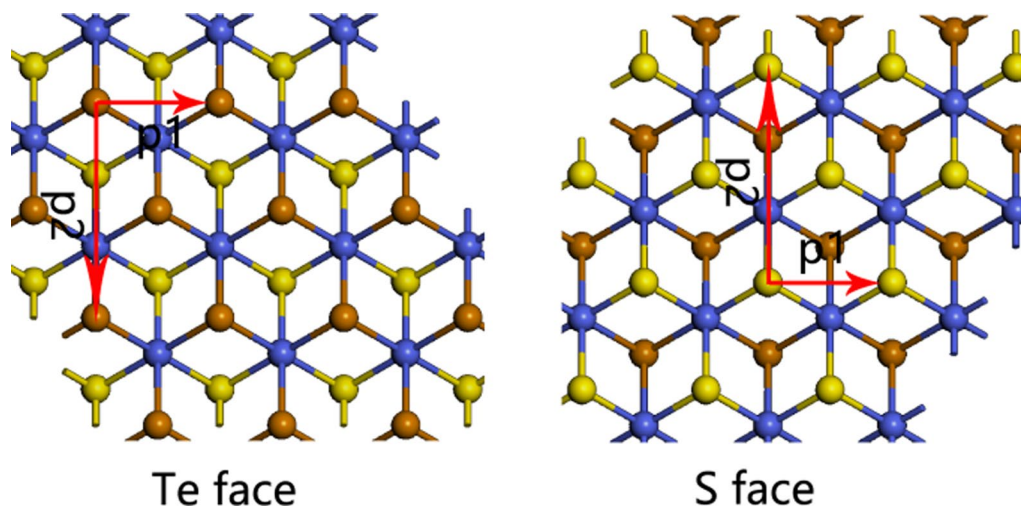

Fig. 6 The diffusion path of Li_2S_n clusters on the surface.

Table III Diffusion energy barrier and diffusion coefficient of S/Te along different paths on the Janus CoSTe monolayer

	Te Path 1	Te Path 2	Te $D2/D1$	S Path 1	S Path 2	S $D2/D1$
Li_2S	0.41	0.49	22.1	0.32	0.39	15.0
Li_2S_2	0.45	0.55	47.9	0.35	0.43	22.1
Li_2S_4	0.53	0.68	331.9	0.50	0.62	103.9
Li_2S_6	0.58	0.86	5.08×10^4	0.56	0.75	1.56×10^3
Li_2S_8	0.64	1.03	3.58×10^6	0.61	0.87	2.34×10^4
Li	0.21	0.25	4.7	0.17	0.20	3.2

barrier in $p2$ direction is generally higher than that in $p1$ direction. In particular, the diffusion coefficient ratio of Li_2S_8 on different paths on the Te surface can reach 10^6 times suggesting that the diffusion of Li_2S_n clusters on the surface of the Janus CoSTe monolayers (especially for high-order Li_2S_n) has a microscopic "channel".

Electronic Structure of the Janus CoSTe Monolayer

It is well known that high conductivity is particularly beneficial to the electrochemical activity during charge/discharge processes. The electronic band structure of the Janus CoSTe monolayer is presented in Fig. 7a. The CoSTe monolayer
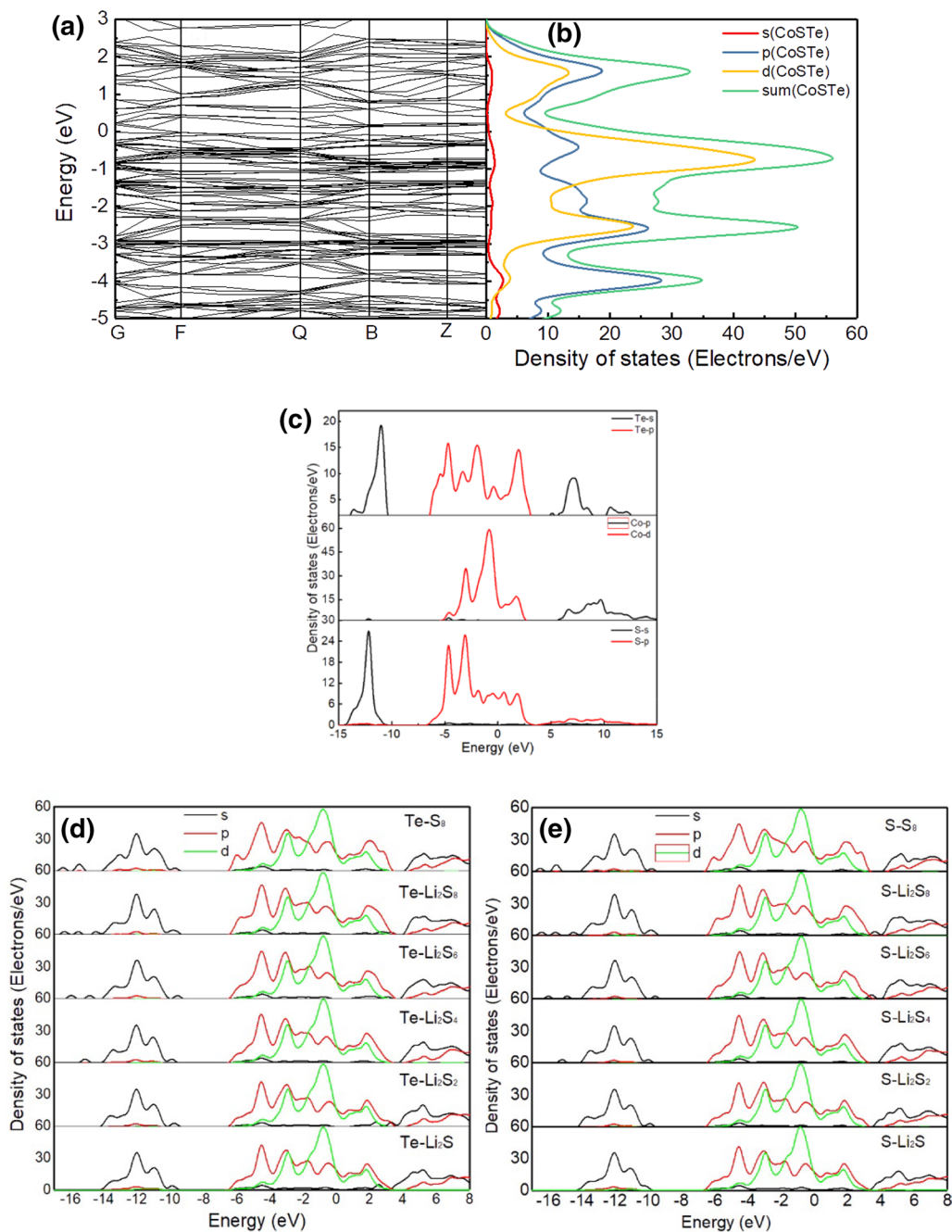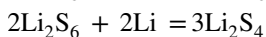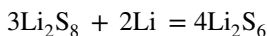

Fig. 7 (a) Band structure diagram and (b) charge density of states near the Fermi surface of the Janus CoSTe monolayer, (c) partial wave density of states of specific atoms, (d) charge density of states of different Li_2S_n clusters adsorbed on the S surface and (e) the Te surface.

exhibits a metallic behavior with zero band gap. The specific charge density distribution is shown in Fig. 7b. The electron orbit near the Fermi surface is occupied, which is mainly contributed by p and d electrons. Figure 7c shows the Janus CoSTe monolayer charge partial wave density of states (PDOS) in which d electrons mainly come from Co atoms, while p electrons mainly come from Te and S atoms, and there is obvious orbital hybridization between p and d electrons. The energy band structure of the Janus CoSTe monolayer after adsorption of S_8 and Li_2S_n clusters is calculated. Figure 7d and e shows the total density of charge states of Li_2S_n clusters adsorbed on Janus CoSTe monolayers. Except for a slight change in quantity, the distribution morphology of charge density of states near the Fermi surface of the monolayers adsorbed S_8 and Li_2S_n clusters is almost unchanged. Thus, the metallic behavior of the monolayer adsorbed S_8 and Li_2S_n clusters can still be well maintained, indicating that the Janus CoSTe monolayer is a good anchoring material for Li-S batteries in terms of electrical conductivity.

Sulfur Reduction on the Janus CoSTe Monolayer During Discharge

During discharge, the chemical reaction between S_8 and Li_2S_n clusters can be described as follows:

$$S_8 + 2Li = Li_2S_8$$
$$3Li_2S_8 + 2Li = 4Li_2S_6$$
$$2Li_2S_6 + 2Li = 3Li_2S_4$$
$$Li_2S_4 + 2Li = 2Li_2S_2$$
$$Li_2S_2 + 2Li = 2Li_2S$$
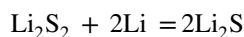
In order to verify the enhanced reaction kinetics by the Janus CoSTe monolayer during discharge, the sulfur reduction reaction (SRR) performance of sulfur on two sides of the Janus CoSTe monolayer was studied.[31] The Gibbs free energy change $\Delta G = \Delta E + \Delta E_{ZPE} - T\Delta S$ before and after the reaction, where ΔE, ΔE_{ZPE} and ΔS are the difference of total energy, zero energy and entropy between the reaction product and the reactant, respectively. Figure 8 shows the Gibbs free energy evolution of each reaction step of sulfur reduction reaction from S_8 to Li_2S on different surfaces. It can be seen that for the two surfaces of the Janus CoSTe monolayer, the first two reduction steps, S_8-Li_2S_8 and Li_2S_8-Li_2S_6, show a spontaneous exothermic reaction, and the three intermediate reaction steps for the subsequent formation of Li_2S_4, Li_2S_2 and Li_2S are endothermic, while the graphite surface is only exothermic from S_8 to Li_2S_8, and the other four intermediate reaction steps are endothermic. For the maximum positive Gibbs free energy change $\Delta G_3 = 0.32$ eV of Te surface corresponds to the step of reduction of Li_2S_6-Li_2S_4, as the rate-limiting step of the whole discharge process, for the S surface and the graphite surface, the maximum
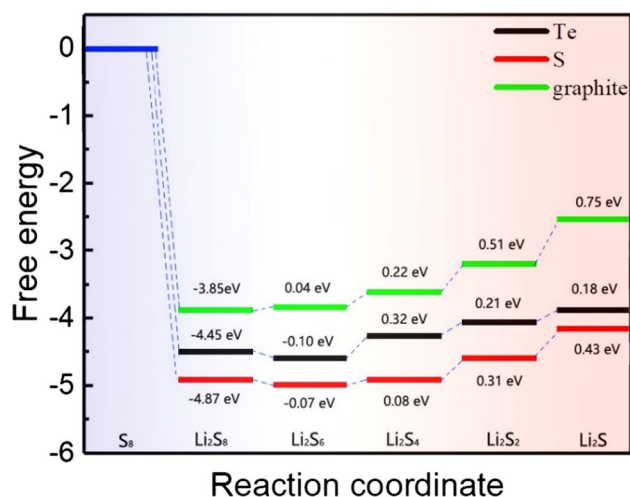

Fig. 8 Gibbs free energy distribution of sulfur reduction on the S/Te surface of the Janus CoSTe monolayer and graphite.

positive Gibbs free energy change ΔG corresponds to the step of Li_2S_2 reduction to Li_2S, which is 0.43 eV and 0.75 eV, respectively, indicating that the formation of solid products is the rate-limiting step of these two surfaces. The Janus CoSTe Gibbs free energy barrier of the two surfaces of the Janus CoSTe monolayer is lower than that of graphite, indicating that the CoSTe monolayer is more favorable for sulfur reduction than that of graphite and can improve the electro chemical performance of Li-S cells.

Charge Transfer Between Li₂S Clusters and the Monolayer

In order to reveal the interaction between Li_2S and CoSTe at a deeper level, the charge difference density diagrams of Li_2S and CoSTe are given, respectively, in Fig. 9. The charge transfer between different atoms can be seen vividly from the charge difference density diagram. In Fig. 9a, several Te atoms close to Li are obviously larger than the red region near the corresponding S atoms in Fig. 9b, indicating that the CoSTe monolayer combines with the Li_2S cluster group. Te can obtain more charge transfer from the Li_2S clusters than the S surface. In Fig. 9c, the blue region that Li atom adsorbed on the Te is smaller than the S surface (Fig. 9d), and the change of the red region around the S atom is not significant, indicating that the charge transfer obtained from the surface comes from the Li atom in the Li_2S clusters.

From the comparison of the change of the density of charge states in Fig. 7d and e, when the Li_2S_n cluster binds to the Te and S surfaces, with the decrease of n, the s-orbital wavelet peak of the low energy level below −15 eV gradually disappears and the s-electron state density of the energy band near the Fermi surface gradually increases. Moreover, the overlap region of p and d electron orbitals increases,
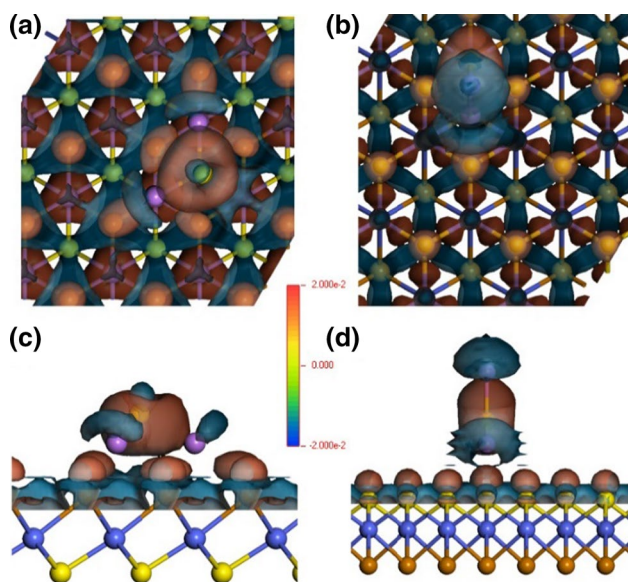
Fig. 9 Charge difference density diagram between Li_2S and surface (red indicates an increase in charge density and blue indicates a decrease), (a) top view of the Te surface, (b) top view of the S surface, (c) side view of the Te surface, (d) side view of the S surface (Color figure online).

indicating that the transition probability of s electrons from low energy level to excited state increases during the evolution from S_8 to Li_2S. The s-, p-, d-orbital hybridization is gradually enhanced, and this complex hybrid mechanism endows the CoSTe surface with a good catalytic effect on the chemical reaction of the Li-S battery.[32]

Conclusion

In summary, the thermodynamically stable structure of the Janus CoSTe monolayer was constructed to investigate the adsorption, decomposition energy, migration path and electronic structure of Li_2S_n clusters on its surface by first-principles calculation. The adsorption and diffusion mechanism of S_8 and Li_2S_n clusters on the Janus CoSTe monolayer was analyzed to study the potential application Li-S cells. The S surface of the Janus CoSTe monolayers shows physical adsorption of sulfiphilicity, which is dominant in the adsorption of high-order Li_2S_n clusters, and the Te surface shows chemical adsorption of lithiophilicity, which accounts for a higher proportion in the adsorption of low-order Li_2S_n clusters. At the same time, the ring structure of the Li_2S_n clusters adsorbed on the two surfaces of the Janus CoSTe monolayer does not decompose, so it can avoid dissolving into the electrolyte. The Li_2S dissociation barriers of Janus CoSTe monolayers are 0.67 eV and 0.74 eV, respectively, which are significantly lower than those of graphite with

1.81 eV. The energy barrier and diffusion coefficient of two diffusion paths perpendicular to each other on the surface are calculated. The results show that the difficulty of Li atom diffusion in different directions on the surface of the Janus CoSTe monolayer is almost the same. The diffusion of Li_2S_n clusters on the S surface of the Janus CoSTe monolayer is easier than that on the Te surface with the same path, and the diffusion difficulty of high-order Li_2S_n clusters is much more difficult than that of low-order Li_2S_n clusters. The diffusion difficulty of Li_2S_n clusters on the same surface is different in different directions, in particularly the diffusion coefficient ratio of Li_2S_8 on different paths of the Te surface can reach 10^6 times. In general, the diffusion of Li_2S_n clusters on the surface of the Janus CoSTe monolayer (especially for the diffusion of high-order Li_2S_n) has a microscopic "channel". The barrier of sulfur reduction reaction on both surfaces of the Janus CoSTe monolayer is lower than that of graphite, which accelerates the formation of the surface Li_2S during discharge, and the maximum reduction energy barrier of the Janus CoSTe monolayer stays in different reaction steps, which is more conducive to the fast reduction reaction. As a result, the Janus CoSTe monolayer shows great potential to be an excellent anchoring material for high-performance Li-S batteries.

References

1. A. Eftekhari and D. Kim, Cathode materials for lithium-sulfur batteries: a practical perspective. *J. Mater. Chem. A* 5, 34 (2017).
2. A. Manthiram, Y. Fu, S.H. Chung, C. Zu, and Y.S. Su, Rechargeable lithium-sulfur batteries. *Chem. Rev.* 114, 23 (2014).
3. G. Minton, M. Wild, M. Marinescu, L. O'Neill, T. Zhang, and R. Purkayastha, Lithium sulfur batteries, a mechanistic review. *Energy Environ. Sci. EES* 8, 12 (2015).
4. Q. Zhang, Y. Wang, Z.W. Seh, Z. Fu, R. Zhang, and Y. Cui, Understanding the anchoring effect of two-dimensional layered materials for lithium-sulfur batteries. *Nano Lett.* 15, 6 (2015).
5. R. Cao, W. Xu, D. Lv, J. Xiao, and J.G. Zhang, Anodes for rechargeable lithium-sulfur batteries. *Adv. Energy Mater.* 5, 16 (2015).
6. X. Lv, W. Wei, H. Yang, J. Li, B. Huang, and Y. Dai, Group IV monochalcogenides MX (*M*=Ge, Sn; *X*=S, Se) as chemical anchors of polysulfides for lithium-sulfur batteries. *Chemistry* 24, 43 (2018).
7. X. Ji and L.F. Nazar, Advances in Li-S batteries. *J. Mater. Chem.* 20, 44 (2010).

8. D.R. Macfarlane, M. Forsyth, P.C. Howlett, M. Kar, and J. Zhang, Ionic liquids and their solid-state analogues as materials for energy generation and storage. *Nat. Rev. Mater.* 1, 2 (2016).

9. H. Peng, J. Huang, and Q. Zhang, A review of flexible lithium-sulfur and analogous alkali metal-chalcogen rechargeable batteries. *Chem. Soc. Rev.* 46, 17 (2017).

10. Y. Song, W. Zhao, L. Kong, L. Zhang, X. Zhu, Y. Shao, F. Ding, Q. Zhang, J. Sun, and Z. Liu, Synchronous immobilization and conversion of polysulfides on a VO_2-VN binary host targeting high sulfur load Li-S batteries. *Energy Environ. Sci.* 11, 9 (2018).

11. Z. Sun, J. Zhang, L. Yin, G. Hu, R. Fang, H. Cheng, and F. Li, Conductive porous vanadium nitride/graphene composite as chemical anchor of polysulfides for lithium-sulfur batteries. *Nat. Commun.* 8, 1 (2017).

12. Y. Zheng, H. Li, H. Yuan, H. Fan, W. Li, and J. Zhang, Understanding the anchoring effect of graphene, BN, C_2N and C_3N_4 monolayers for lithium-polysulfides in Li-S batteries. *Appl. Surf. Sci.* 434, 596 (2018).

13. Z. Chang, B. Ding, H. Dou, J. Wang, G. Xu, and X. Zhang, Hierarchically porous multilayered carbon barriers for high-performance Li-S batteries. *Chemistry* 24, 15 (2018).

14. J. Li, J. Guo, J. Deng, and Y. Huang, Enhanced electrochemical performance of lithium-sulfur batteries by using mesoporous TiO_2 spheres as host materials for sulfur impregnation. *Mater. Lett.* 189, 100526 (2016).

15. R. Ponraj, A.G. Kannan, J.H. Ahn, and D.W. Kim, Improvement of cycling performance of lithium-sulfur batteries by using magnesium oxide as a functional additive for trapping lithium polysulfide. *ACS Appl. Mater. Interfaces* 8, 6 (2016).

16. Y. Tao, Y. Wei, L. Yu, J. Wang, and D. Long, Kinetically-enhanced polysulfide redox reactions by Nb_2O_5 nanocrystals for high-rate lithium-sulfur battery. *Energy Environ. Sci.* 9, 10 (2016).

17. Y. Xu, X. Ou, and X. Zhang, Theoretical study of two-dimensional α-tellurene with pseudo-heterospecies as a promising elemental anchoring material for lithium-sulfur batteries. *J. Phys. Chem. C* 125, 8 (2021).

18. W. Yin, B. Wen, G. Nie, X. Wei, and L. Liu, Tunable dipole and carrier mobility for a few layer Janus MoSSe structure. *J. Mater. Chem. C* 6, 7 (2018).

19. I.D. Muhammad, M. Awang, O. Mamat, and Z.B. Shaari, First-principles calculations of the structural, mechanical and thermodynamics properties of cubic zirconia. *World J. Nano Sci. Eng.* 04, 02 (2014).

20. J.P. Perdew, K. Burke, and M. Ernzerhof, Generalized gradient approximation made simple. *Appl. Phys. Lett.* 77, 18 (1996).

21. M.D. Segall, P.J.D. Lindan, M.J. Probert, C.J. Pickard, P.J. Hasnip, S.J. Clark, and M.C. Payne, First-principles simulation: ideas, illustrations and the CASTEP code. *J. Phys. Condens. Matter* 14, 11 (2002).

22. X.F. Jia, Q.Y. Hou, Z.C. Xu, and L.F. Qu, Effect of Ce doping on the magnetic and optical properties of ZnO by the first principle. *J. Magn. Magn. Mater.* 465, 128 (2018).

23. T.H. Fischer, and J. Almlof, General methods for geometry and wave function optimization. *J. Phys. Chem.* 96, 24 (1992).

24. Y. Ding, M. Chen, and W. Wu, Phase stability, elasticity, hardness and the minimum thermal conductivity of Si_2N_2O polymorphs from first principles calculations. *Phys. B Condens. Matter* 449, 236 (2014).

25. T. Zhou, W. Lv, J. Li, G. Zhou, Y. Zhao, S. Fan, B. Liu, B. Li, F. Kang, and Q. Yang, Twinborn TiO_2-TiN heterostructures enabling smooth trapping–diffusion–conversion of polysulfides towards ultralong life lithium-sulfur batteries. *Energy Environ. Sci.* 10, 7 (2017).

26. S. Grimme, J. Antony, S. Ehrlich, and H. Krieg, A consistent and accurate ab initio parametrization of density functional dispersion correction (DFT-D) for the 94 elements H-Pu. *J. Chem. Phys.* 132, 15 (2010).

27. H. Zhang, S. Wang, Y. Wang, B. Huang, Y. Dai, and W. Wei, Borophosphene: a potential anchoring material for lithium-sulfur batteries. *Appl. Surf. Sci.* 562, 150157 (2021).

28. A. Ww, A. Yz, A. Yg, A. Jb, A. Cz, A. Zc, A. Yl, and B. Bx, Exploring anchoring performance of InP3 monolayer for lithium-sulfur batteries: a first-principles study. *Appl. Surf. Sci.* 526, 146717 (2020).

29. G. Zhou, H. Tian, Y. Jin, X. Tao, B. Liu, R. Zhang, Z.W. Seh, D. Zhuo, Y. Liu, J. Sun, J. Zhao, C. Zu, D.S. Wu, Q. Zhang, and Y. Cui, Catalytic oxidation of Li_2S on the surface of metal sulfides for Li-S batteries. *Proc. Natl. Acad. Sci.* 114, 5 (2017).

30. R.A. Olsen, G.J. Kroes, G. Henkelman, A. Arnaldsson, and H. Jónsson, Comparison of methods for finding saddle points without knowledge of the final states. *J. Chem. Phys.* 121, 20 (2004).

31. Z. Du, X. Chen, W. Hu, C. Chuang, S. Xie, A. Hu, W. Yan, X. Kong, X. Wu, H. Ji, and L. Wan, Cobalt in nitrogen-doped graphene as single-atom catalyst for high-sulfur content lithium-sulfur batteries. *J. Am. Chem. Soc.* 141, 9 (2019).

32. Z. Han, R. Gao, Y. Jia, M. Zhang, Z. Lao, B. Chen, Q. Zhang, C. Li, W. Lv, and G. Zhou, Catalytic effect in Li-S batteries: from band theory to practical application. *Mater. Today* 24, 57 (2022).